Mechanics Based Design of Structures and Machines

An International Journal

ISSN: 1539-7734 (Print) 1539-7742 (Online) Journal homepage: https://www.tandfonline.com/loi/lmbd20

Modeling and Analysis of Vibration-Induced Changes in Connector Resistance of High Power Electrical Connectors for Hybrid Vehicles

Rujian Fu , Song-Yul Choe , Robert L. Jackson , George T. Flowers & Daegee Kim

To cite this article: Rujian Fu , Song-Yul Choe , Robert L. Jackson , George T. Flowers & Daegee Kim (2012) Modeling and Analysis of Vibration-Induced Changes in Connector Resistance of High Power Electrical Connectors for Hybrid Vehicles, Mechanics Based Design of Structures and Machines, 40:3, 349-365, DOI: 10.1080/15397734.2012.670098

To link to this article: https://doi.org/10.1080/15397734.2012.670098

Published online: 05 Jul 2012.

Mechanics Based Design of Structures and Machines, 40: 349–365, 2012

ISSN: 1539-7734 print/1539-7742 online
DOI: 10.1080/15397734.2012.670098

MODELING AND ANALYSIS OF VIBRATION-INDUCED CHANGES IN CONNECTOR RESISTANCE OF HIGH POWER ELECTRICAL CONNECTORS FOR HYBRID VEHICLES[#]

Rujian Fu[1], Song-Yul Choe[1], Robert L. Jackson[1], George T. Flowers[1], and Daegee Kim[2]

[1]*Department of Mechanical Engineering, Auburn University, Auburn, Alabama, USA*

[2]*LS Cable Company, Ltd., South Korea*

High power connectors used in hybrid vehicles are exposed to vibrations that cause changes in connector resistance. When vibration starts, the connector resistance increases temporarily and oscillates. When vibration stops, the connector resistance returns to a value that is similar to the original state. In this paper, finite element models are developed to analyze this phenomenon and compared with experimental results. A two-dimensional finite element model was developed to predict the motions at any location of the connector system. A contact spring present between the female and male parts of the connector is modeled in three dimensions and used to analyze the time response. The analysis shows that the relative displacement is closely related to the changes of connector resistance during vibration, and the models can be used to improve connector design and ensure better performance and reliability.

Keywords: Contact resistance; Finite element modeling; Fretting; High power connector; Round pin connector; Vibration.

INTRODUCTION

Hybrid electric propulsion systems are the platform for the future propulsion systems that substantially increase fuel economy and reduce emissions. However, there are technical barriers that prevent its success. One of the crucial technical problems with the hybrid systems is the lack of reliability of the electrical components. The electrical components should be guaranteed for the same period of time as the mechanical components.

Typical hybrid systems use one or two electric motors that are mechanically connected to shafts and electrically connected to batteries via DC/AC inverters and a DC/DC converter. The DC/DC converter is usually located in the rear trunk area, while the motors and DC/AC inverters are located in the engine compartment. Therefore, the electrical power connectors have different electrical and mechanical

Received February 13, 2011; Accepted August 19, 2011
[#]Communicated by J. McPhee.
Correspondence: Rujian Fu, Department of Mechanical Engineering, 1418 Wiggins Hall, Auburn University, Auburn, AL 36380, USA; E-mail: rzf0007@tigermail.auburn.edu

specifications. Their voltage and current ratings, as well as ambient temperature and vibrations, are dependent on their locations.

Connectors in hybrid systems are exposed to a harsh automobile environment where temperature, humidity, vibration frequency, and amplitude vary. These harsh conditions are induced by engine operation and motion of the vehicle. Particularly, vibrations induce the degradation of connectors, which is regarded as fretting. Fretting is defined as a relative cyclic motion with small amplitude that occurs between two oscillating surfaces (Waterhouse, 1972). It is also characterized in terms of the local relative motion (Varenberg et al., 2004). The fretting causes wear and corrosion on the contact materials, which results in a gradual increase of contact resistance. However, it is also observed that the temporary changes of contact resistance are superimposed on the gradual increases. Various studies showed that the contact resistance may increase temporarily and significantly, and then oscillate synchronously with the vibration (Carvou and Jemaa, 2007, 2009; Hubner-Obenland and Minuth, 1999; Jemaa, 2002; Kopanski, 1998; Malucci, 2000; Maul et al., 2001; Maul and McBride, 2002; McBride, 1989; Murrel and McCarthy, 1997; Skinner, 1975).

This vibration-induced change of contact resistance is caused by various mechanisms. Some authors found the change related to the wear debris and particles at the contact surfaces (Carvou and Jemaa, 2007; Hubner-Obenland and Minuth, 1999; Skinner, 1975). Some explained it as an intermittence phenomenon, which describes the variation of contact resistance associated with short duration discontinuities of the contacts (Malucci, 2000; Maul et al., 2001; Maul and McBride, 2002; Murrel and McCarthy, 1997). Other researchers found that the periodic separations of contact surface, or contact gaps, also have major effects on the temporary increases and oscillations of the contact resistance (Kopanski, 1998; McBride, 1989; Yan et al., 2005). This phenomenon is commonly found on electrical connectors subject to vibration, as well as relays and switches, which may cause electrical arcing. A mathematical model of the contact bounce is developed to show that the contact separations are small such that the minimum arc voltage is reached (McBride, 1989). It is found that the electrical arcing causes contact resistance to enhance progressively and demonstrates high fluctuations during vibrations (Carvou and Jemaa, 2009; Jemaa, 2002). The arcing voltage may also be caused by a bounce phenomenon between the contacts during vibrations (Carvou and Jemaa, 2009). In addition, the periodic separation of contact surfaces changes the capacitance between the contacts, which was measured for a lithographic overlay subject to vibration (Kopanski, 1998).

Most research conducted in the past focused on low power connectors, for which the current ratings are less than hundreds of milliamps. In our previous work (Fu et al., 2012), the high power connectors, which have round type pins with a current rating of 300A, were investigated experimentally. The results showed that the connector resistance suddenly increased and oscillated when a vibration was applied and returned back to the normal state when vibration stopped. In this paper, we investigate the mechanism involved in this phenomena caused by the periodic gaps between contact surfaces using finite element models.

Analytical modeling could help understand the nature of intermittent contact due to vibration. An elastic structure subject to vibrations with intermittent contact was analytically modeled using Euler–Bernoulli beam theory (Ervin and Wickert,

2007). To analyze structures with complicated geometries, some other authors used finite element methods (FEM) (Angadi et al., 2012; Chen et al., 2009; Polchow et al., 2010; Spitas and Spitas, 2007; Xie et al., 2009; Zhai et al., 2006). FEM was used to predict resistance, temperature and stress for high power connectors based on the multi-physics mechanism of structural, thermal and electrical effects (Angadi et al., 2012; Polchow et al., 2010). Some authors used FEM for analysis of dynamics and fretting of connectors subjected to vibration (Chen et al., 2009; Xie et al., 2009). FEM was also used for analysis of the dynamic characteristics of the pick-up and drop-out process of the contact in an electromagnetic relay (Zhai et al., 2006). However, computational time of FEM increases drastically to calculate dynamic characteristics of connectors using a three-dimensional model (Chen et al., 2009). Thus, to minimize the computational cost, we developed a two-dimensional model for the connector system that embeds a detailed three-dimensional model for the contact spring. The model is used to analyze the effects of vibrations on the contact surfaces. Experiments are used to verify the numerical analysis.

EXPERIMENTAL RESULTS OF CONNECTORS

Specification for the High Power Connectors

Connectors used for experiments are made of male and female parts connected by a spring that allows for the absorption of mechanical vibrations while maintaining high conductance, as shown in Fig. 1. The connector has an axis-symmetric cylindrical shape. The male part has a pin with a round shape [Fig. 1(d)], while the female part has a tube form [Fig. 1(b)]. A ring-shaped spring punched from a sheet metal is mounted inside the female part [Fig. 1(c)]. The spring serves to produce contact pressures perpendicular to the surface of the male and female parts by contact tabs. The contact pressures compress each contact tab in the radial direction and provide electrical connections between the male and female parts of the connector. The specifications of the 300A rated connector used in this study, as well as the material properties, are listed in Table 1. The connector surface is plated with silver, while the bulk connector material is made of copper alloy.

Design of Test Stand

In order to study the effects of vibration on connectors, a test station was designed and fabricated to facilitate the generation of vibrations, supply of a high current, and measurement of connector resistance and motion. Using digital data acquisition hardware and software, the measured data were processed and displayed. A schematic diagram of the designed test stand is depicted in Fig. 2.

The shaker used for generating vibrations in our experiments was a LDS^{TM} V850 electro-dynamic shaker, onto which a connector was mechanically fixed. The connector system also included a housing on the female part and a supplied cable connected to the male part, as shown in Fig. 3. Fixture clamps were used to firmly hold the left end of the connector housing and the right end of supplied cable to the shaker. The direction of applied vibration was perpendicular to the cable.

The connector resistance was calculated by the measurements of voltage and current, where a high accurate current sensor was used. The resolution of the

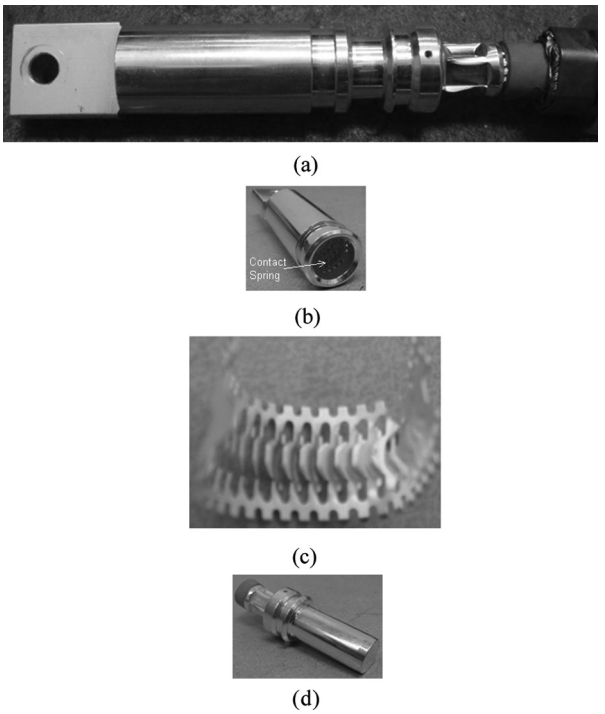

Figure 1 Geometrical structures of the connector: (a) connector mate, (b) female part with contact spring, (c) contact spring, and (d) male part (color figure available online).

resistance theoretically reaches $0.02\,\mu\Omega$, so the effects of vibrations on the change of resistance were detected with a high precision. The locations for measurement of R_C are shown in Fig. 3.

U_0, U_1, U_2, and U_3 are the displacements measured on the fixture clamp, the female part, the right end of male part, and the midpoint of the supplied

Table 1 Specifications of the connector

Components	Male part, female part and contact spring
Material properties	
Bulk material	Copper alloy
Young's modulus (GPa)	117
Poisson's ratio	0.34
Mass density (kg/m^3)	8930
Surface plating	silver
Friction coefficient	0.34
Dimensions	
Overall length (mm)	105.3
Outer diameter (mm)	20.1
Current rating (A)	300

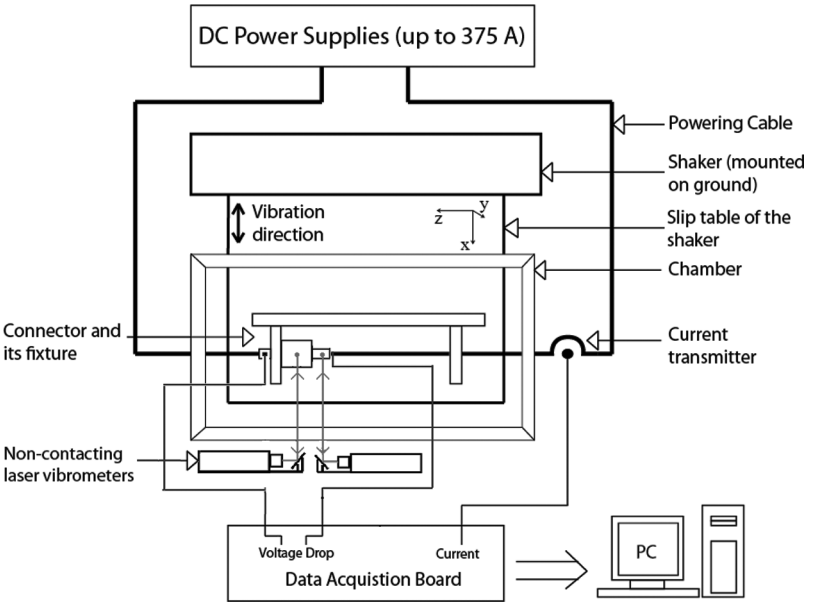

Figure 2 A schematic diagram of the test stand (color figure available online).

cable respectively, as shown in Fig. 3. The measurement of the displacements was carried out using two non-contacting laser vibrometers, as shown in Fig. 2. U_0 was measured by one vibrometer and taken as the excitation and reference. The responses at three other locations, U_1, U_2, and U_3, were measured by the other vibrometer, which provide the magnitude and phase of each motion based on the reference. Each motion is given as a polar form in the following equation:

$$U_i = M_i \sin(\omega t + \varphi_i) = M_i \angle \varphi_i \tag{1}$$

where M_i is the magnitude and φ_i is the phase shift of the motion U_i.

Experimental Results

The test conditions are shown in Table 2. The amplitude of vibrations was set to a constant value of 0.18 mm, while the frequency was changed from 20 Hz

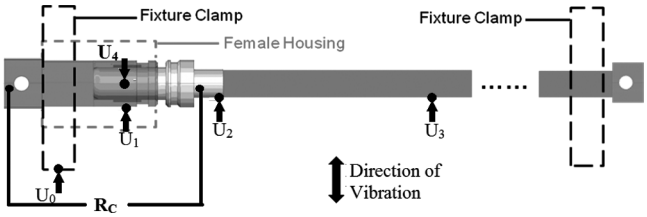

Figure 3 The connector system and measurement locations of motions and connector resistance (color figure available online).

Table 2 Test conditions

Amplitude	Frequency	Duration	Current	Temperature
0.18 mm	20 Hz, 40 Hz, ... , 220 Hz, 240 Hz	2 min for each frequency	80 A DC	Room temperature

to 240 Hz with an incremental step of 20 Hz. Every vibration lasted 2 min at each frequency with a pause of 1 min. The tests were conducted under the flow of a constant DC current of 80 A and at room temperature.

The amplitude of the motions, M_0 through M_3, and the connector resistance, R_C, were measured in real time during vibration. Since the connector was fixed on the shaker, it is assumed that U_0 is same as the excitation of the shaker. The magnitude ratios of the motions (M_1/M_0, M_2/M_0, and M_3/M_0) obtained in experiments are plotted as dots in Fig. 7. M_1 was measured at the female part and it increased slightly when the frequency increases, as shown in Fig. 7(a). M_2 was measured at the right end of male part and it increased significantly at 60 Hz and 220 Hz, which indicates resonances that took place at the two frequencies, as shown in Fig. 7(b). M_3 was measured at the middle point of power cable and it increased significantly at 60 Hz, which indicates that a resonance took place at the frequency, as shown in Fig. 7(c).

Figure 4 shows the R_C before, during and after the vibration at 220 Hz. As vibration started, the R_C increased suddenly and oscillated until the vibration ended. When the vibration stopped, the R_C decreased and remained at a value that was close to the value before application of the vibration. In order to characterize the effects of the vibration on the change of resistance, an average value of change of the R_C during vibration, ΔR_C, is defined and shown in Fig. 4 and then used as a new criterion for assessing the effects. Measured ΔR_C as a function of frequencies is shown as dots in Fig. 9. Generally, the connector resistance increased as the

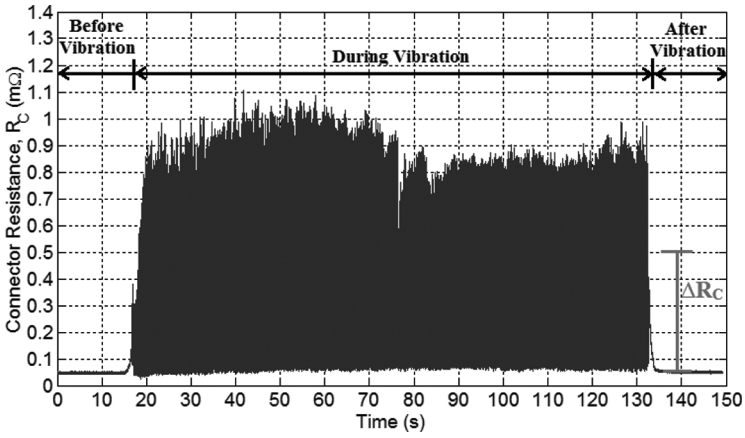

Figure 4 Connector resistance during vibration (amplitude = 0.18 mm, frequency = 220 Hz, g-value = 17.5) (color figure available online).

frequency increased. The value reached the peaks at two resonant frequencies, which will be theoretically verified using the developed model.

MODELING OF THE CONNECTOR SYSTEM BY FEM

The experimental results obtained in the previous paper (Fu et al., 2012) showed that the ΔR_C is mainly affected by the relative displacement between the right end of the male and the female part, $|U_2 - U_1|$. In fact, $|U_2 - U_1|$ is different from the relative displacement at the contact surface between the male (U_4) and the female part (U_1) of the connector. In this paper, we developed a vibration model to predict U_4, as shown in Fig. 3, since U_4 is not accessible for the measurement. As a result, the model allows for an accurate analysis of the effects of the relative displacement $|U_4 - U_1|$ on the ΔR_C.

Set-Up

A schematic of the model mesh and boundary conditions are shown in Fig. 5, where the connector system shown in Fig. 3 is separated into four different components: a female part with the housing, a male part, a supplied cable, and a contact spring. The female part with the housing is regarded as a mass that is shaped to enclose the male part and contact spring. The male part and the cable are approximated by two beams that attach to each other, whose material properties and dimensions are shown in Table 3.

Using the commercial finite element software, ANSYS™, the four components mentioned above are modeled by a two-dimensional structure using one-dimensional elements. The connector and cable are modeled using beam element, Beam3, where all the material properties and the real constants are used for input variables. The contact spring is modeled using the spring-damper element, the Combin14, where a spring constant and a damping ratio are needed. The details of how to determine the spring constant is explained in section III-B.

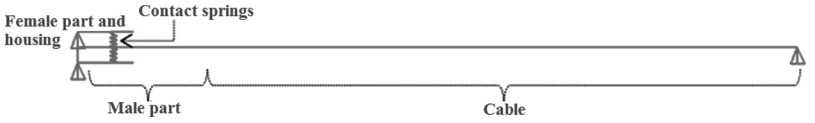

Figure 5 Finite element model for the connector system with boundary conditions (color figure available online).

Table 3 Material and dimensional properties of male part and cable

	Connector (copper alloy)	Cable (composite material of strands and shielding)
Young's modulus (GPa)	117	3.3
Mass density (kg/m^3)	8930	2506
Length (mm)	60	270
Cross-section area (mm^2)	150	200

Once the element types and the material properties are chosen, boundary conditions for the nodes of elements are applied. The nodes on the fixture clamps are fixed to the excitation and marked with small triangles, as shown in Fig. 5. Also, it is assumed that the displacements of all nodes are in the same direction as that of the excitation, so no nodes are vibrating in the axial direction and the corresponding displacements can be set to be zero.

Determination of the Equivalent Spring Constant

The ring-shaped spring located between the male and female parts is approximated with two simple equivalent springs. The spring has 22 repeated sections that are uniformly distributed around the circumference and in contact with the female part on one side and male part on the other side, as shown in Figs. 1(b) and (c). Each section of spring consists of tabs connected over a bridge and is compressed in the radial direction by the male part. The 22 repeated sections are regarded as 22 linear springs that can be reduced to two springs under an assumption that the displacement of the male part is only in the direction of excitation.

The spring constant, k_e, is derived from the relationship between force and displacement. This relationship for a single section of the spring is attained from a three-dimensional static finite element simulation using the model described in Section IV. For the ith repeated section, the relationship is calculated as

$$F_{r,i} = 24r_i + 8 \tag{2}$$

where r_i is the radial displacement of the ith spring from a steady state position (mm), and $F_{r,i}$ is the radial contact force (N). The linear equation above includes an unknown variable, r_i. When the male part moves in the vibration direction by d, which is known as the relative displacement between the male and female parts, r_i changes accordingly. As shown in Fig. 6(a), r_i can be expressed as a function of d from the triangle QOP, as shown in equation (3):

$$r_i = d\cos\alpha_i - R + \sqrt{R^2 + d^2(\cos^2\alpha_i - 1)} \tag{3}$$

where R is the radius of the male part (mm) and α_i is the angle from the x direction to the radial direction of the ith spring.

Hence, the contact force in the radial direction for the ith spring is obtained from equations (2) and (3). The force, $F_{r,i}$, can be decomposed into two components, $F_{x,i}$ and $F_{y,i}$, as shown in Fig. 6(b), where the x represents the direction of the vibration. The sum of all forces exerted in the y direction is zero because the problem is symmetric when the male part vibrates in the x direction. The resultant contact force, F_x, can be expressed as follows:

$$F_x = \sum_{i=1}^{22} F_{x,i} = \sum_{i=1}^{22} F_{r,i}\cos\alpha_i \tag{4}$$

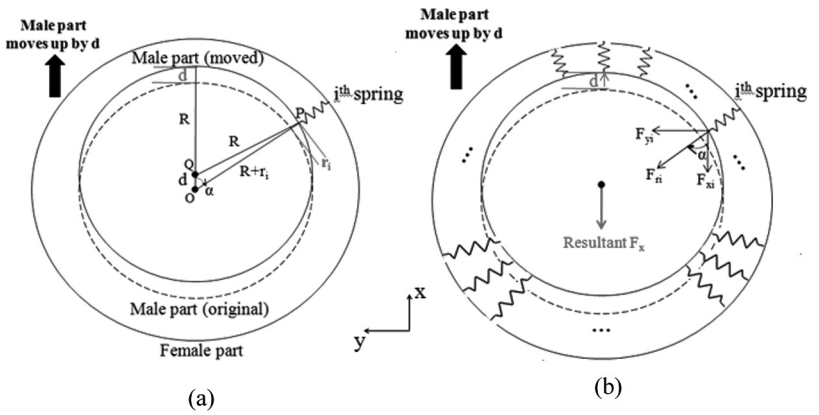

Figure 6 Schematic diagrams for calculation of an equivalent spring constant. (a) Calculation of the radial displacement for the ith spring. (b) Calculation of the resultant force in X direction (direction of vibration) (color figure available online).

Consequently, the equivalent spring constant k_e for the two simplified linear springs can be calculated by:

$$k_e = \frac{F_x}{2d} = \frac{\sum_{i=1}^{22}\left[24\left(d\cos\alpha_i - R + \sqrt{R^2 + d^2(\cos^2\alpha_i - 1)}\right) + 8\right]\cos\alpha_i}{2d} = 257\,\mathrm{N/mm} \tag{5}$$

In this way, the spring constant for the spring element, Combin14, is determined. The friction between the spring and both male and female parts of connector are neglected in this model.

Comparison Between Simulation and Experimental Results

The vibration model developed above is compared with experimental results. The frequency and amplitude of the excitation used for the simulation are same as the experiments, as shown in Table 2, where the marked small triangle in Fig. 5 indicates the two excited points on the female parts and one point at the end of cable. Like the experimental set-up, U_0 presents the displacement at the reference point. U_1, U_2, U_3, and U_4 are the displacements at different points that are predicted by the simulation.

A comparison between simulations and experiments is shown in Fig. 7(a)–(c) at different locations, where the magnitude ratios of $M_1/M_0 \sim M_3/M_0$ are plotted. The results show a reasonable match between simulations and experiments in M_1 and M_2, but a deviation around a resonance peak is observed at M_3. Since U_4 is inaccessible for measurement, only simulations are carried out and their results are plotted in Fig. 8, where the ratio of the magnitude increases at two resonance frequencies of around 60 Hz and 190 Hz.

Based on the previous results, the relative displacements between the male and female parts at the contact surfaces are studied. The relative displacement, d,

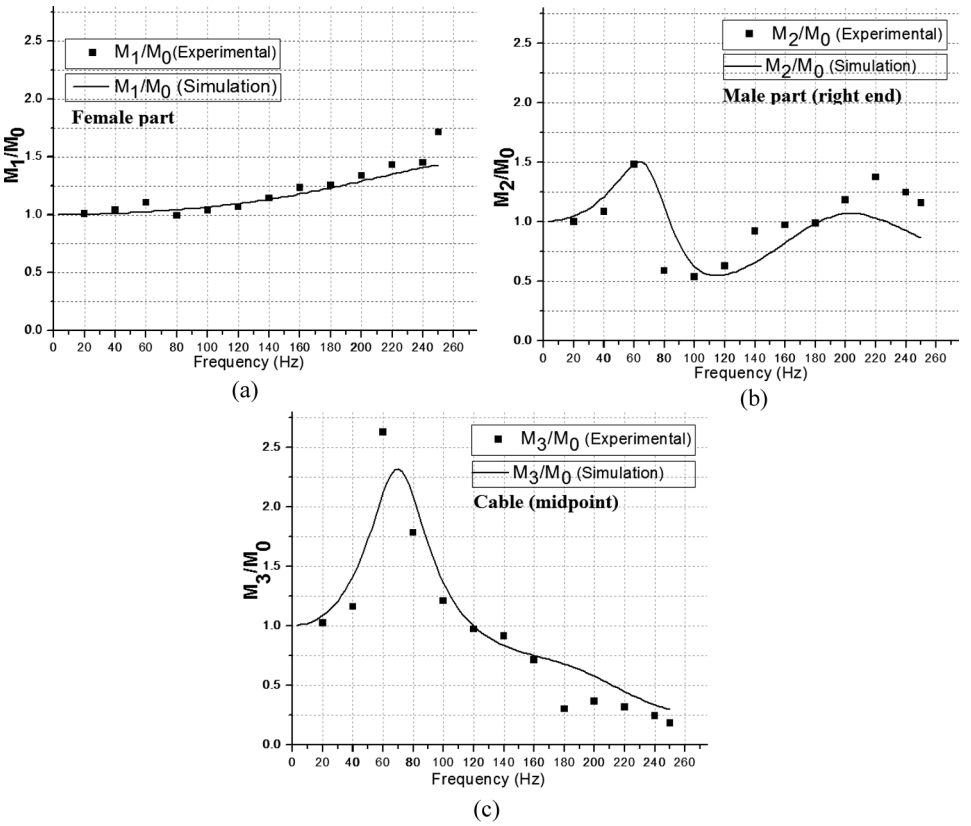

Figure 7 Comparison between simulated and experimental results. (a) The magnitude of the female part (M_1) versus the excitation (M_0). (b) The magnitude of the right end of male part (M_2) versus the excitation (M_0). (c) The magnitude of the midpoint of cable (M_3) versus the excitation (M_0).

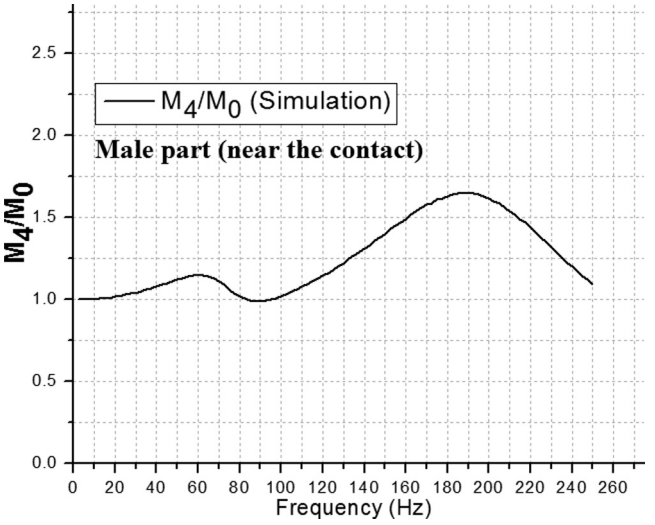

Figure 8 Simulation result: The magnitude of the male part (near the contact) (M_4) versus the excitation (M_0).

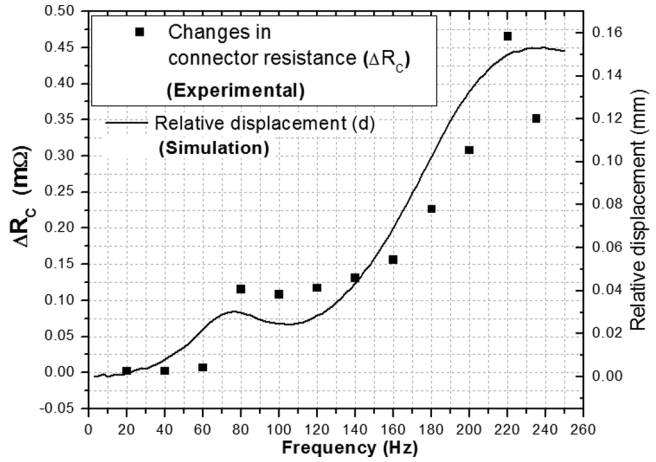

Figure 9 Comparison between relative displacement (simulation) and changes of *n* connector resistance (experiment).

is defined as an absolute value of the difference between U_4 and U_1, as follows in equation (6):

$$d = |U_4 - U_1| = M_1\sqrt{\left(1 - \frac{M_4}{M_1}\cos(\varphi_4 - \varphi_1)\right)^2 + \left(\frac{M_4}{M_1}\sin(\varphi_4 - \varphi_1)\right)^2} \qquad (6)$$

where M_1, M_4, φ_1, and φ_4 are calculated using the model.

The simulated relative displacement, d, and the change of experimentally measured connector resistance, ΔR_C, at different excitation frequencies are plotted in Fig. 9. The plot shows a relatively good correlation between the magnitudes at the two resonant frequencies that are located at 80 Hz and 220 Hz, which implies that the change of connector resistance is affected by the relative displacement at the contact surfaces. These relative displacements could form gaps between the contact surfaces that increase connector resistance, which is analyzed in the following section.

MODELING OF THE CONTACT SPRING BY FEM

In order to clearly explain the correlation mentioned above, a three-dimensional model for one repeated section of the contact spring is developed using ANSYS™ and used to analyze the time response of vibrations.

Set-Up

The geometry and mesh for the model is shown in Fig. 10. Since the connector is axis-symmetric for its cylindrical shape and the spring is periodic, only a part of the connector is considered for the modeling. The connector model includes one surface of the female and the male parts as well as a repeated section of spring.

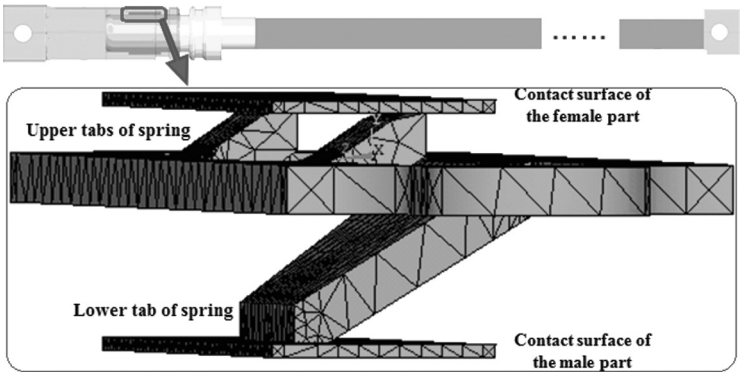

Figure 10 Finite element model of one repeated section of contact spring (color figure available online).

According to the actual geometry shown in Fig. 1(c), the repeated section of spring has two upper contact tabs and one lower contact tab connected by a bridge.

In order to perform the structural analysis of the bulk materials, the element of Solid187 is used, which is a high order three-dimensional element with 10 nodes, while Targe170 elements and Conta174 elements are needed for analysis of the three pairs of contacting surfaces. The three contact pairs present two upper tabs and one lower tab. The material properties of the bulk material and the contact pairs are given in Table 1. Interference of contact is considered to include the effect of preload in static state before applying vibrations.

The displacement boundary conditions for the individual spring model are obtained from the previous simulation, as shown in Fig. 9. When the connector vibrates, the female and male parts oscillate. To simplify the following boundary conditions, the female part is regarded as fixed while the male part oscillates with the amplitude of the relative displacement, $|U_4 - U_1|$. Symmetric boundary conditions are also applied on the repeated section of the contact spring. In addition, it is assumed that only displacements in the direction of vibration are allowed on the sides of the spring.

RESULTS

The model developed above is used to study time responses of displacements of the spring at four locations: the lower tab of the spring, the upper tabs of the spring, the contact surface of the female part and the contact surface of the male part, as shown in Fig. 10. Simulations can be run for different cases, so that a case is selected from the data shown in Fig. 9, where the relative displacement is 0.153 mm at the excitation frequency of 220 Hz. Eight full periods of the vibration are applied to study the steady state response, as shown in Fig. 11.

The displacements of the lower tab of the spring and the male part are shown in Fig. 11(a), where the displacement of the lower tab irregularly varies when vibration is applied and appears to reach a steady state after the second cycle of vibration. In the steady state, the overlapping of two lines indicates that they are in contact. However, contact gaps are formed periodically when the male part reaches

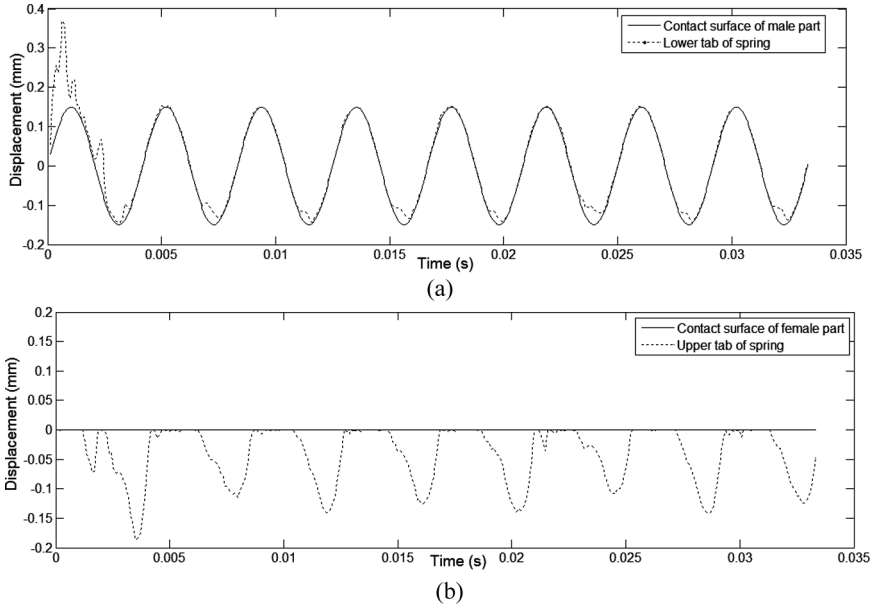

Figure 11 Time response of the displacements versus time when excitation frequency equals to 220 Hz.

the minimum displacement values in each cycle. Therefore, contact between the male part and the spring is not continuous.

The response of the upper tabs and the female part are shown in Fig. 11(b), where the displacement of the upper tab irregularly varies at the beginning and reaches an approximate steady state after the second cycle of vibration. In the steady state, a gap between the upper tabs of the spring and the contact surface of the female part is produced during each period. Therefore, the contact between the female part and the spring is not continuous as well. The intermittent contact could be the cause of the temporary increase in contact resistance that is observed experimentally.

The occurring gaps explained above are now depicted using the three-dimensional FEM images. Three deformed shapes of the spring at different instances are shown in Fig. 12. When the second cycle starts at $t = 0.0043$ sec, the shape of the spring shows that it is located at the equilibrium position and that no contact gap is observed, as shown in Fig. 12(a). At $t = 0.0050$ sec, the male part presses the spring, so that the lower tab loses contact with the male part, as shown Fig. 12(b). At $t = 0.0070$ sec, the spring loses contact with the female part as well as the male part, as shown in Fig. 12(c). The color bar in Fig. 12(d) indicates the displacement of each finite element node.

Similarly, studies are performed for two more cases at 160 Hz and 60 Hz. Displacements between two contacts at the second period of vibration are shown in Fig. 13. The gap produced is smaller at 160 Hz compared to that of 220 Hz. At 60 Hz, the gap becomes negligible. The analysis shows that the gaps between contact surfaces vary with vibration frequency and they become larger under higher relative displacement, which appears to be the cause of the temporary changes in the connector resistance.

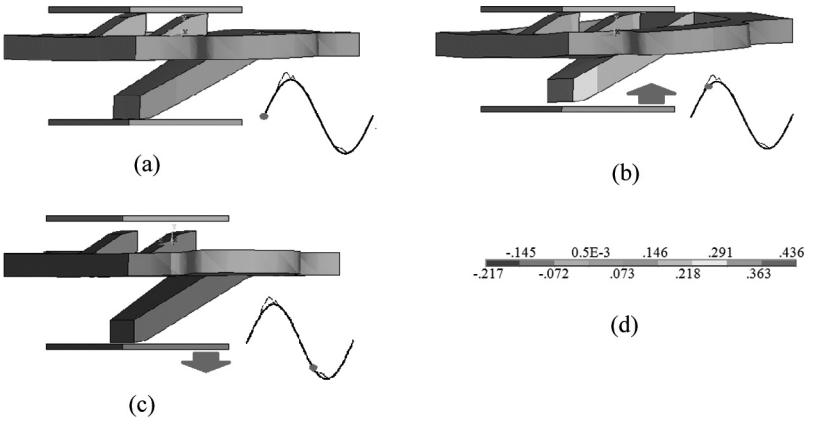

Figure 12 The deformed shapes at different moments, corresponding to Fig. 11: (a) deformed shape at the rate of $t = 0.0043$ sec, around equilibrium position, (b) deformed shape at the rate of $t = 0.0050$ sec, male part moving up, (c) deformed shape at the rate of $t = 0.0070$ sec, male part moving down, and (d) color bar showing the nodal displacement (mm) (color figure available online).

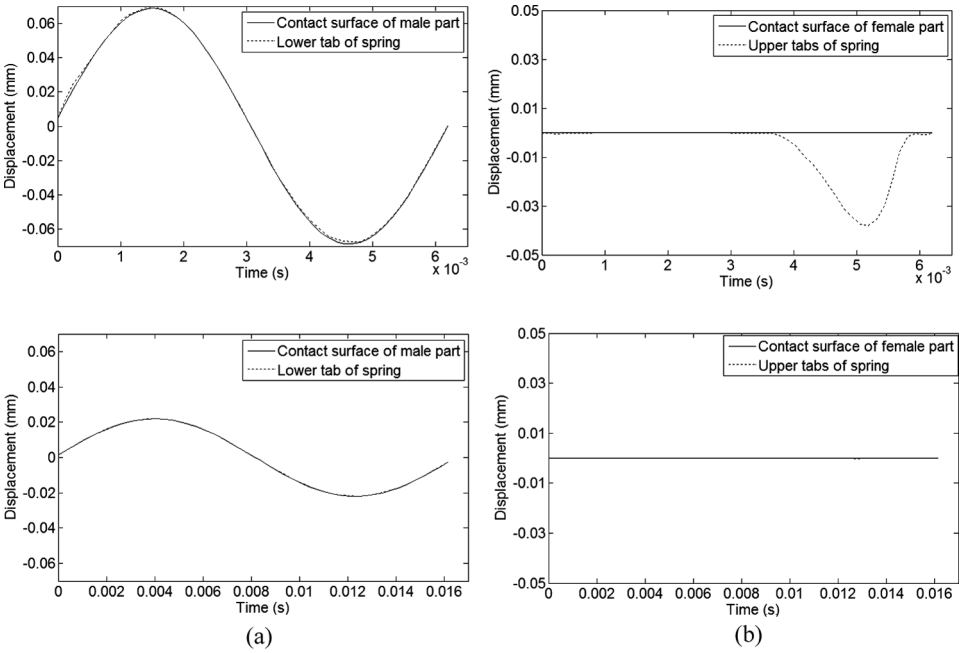

Figure 13 Time response of the displacements versus time at excitation frequency of (a) 160 Hz and (b) 60 Hz.

CONCLUSIONS

In this paper, we theoretically studied the responses of a high power connector subject to vibrations based on a two-dimensional FEM model for the connector

system and a three-dimensional FEM model for a section of the contact spring. The two-dimensional model is used to calculate the relative displacement between the male and female part of the connector at contact, which directly affects the changes of connector resistance measured in experiments. The model is validated with experimental results.

The spring used for this high power connector has a complex shape, whose behavior during vibration is difficult to predict. Thus, the three-dimensional model is used to calculate time responses of the spring subject to vibration, which induces the contact gaps and consequently change the contact resistance.

The major findings are summarized as follows:

1. When a connector is exposed to vibrations, the connector resistance significantly increases and oscillates. When the vibrations are stopped, the resistance returns to a value that is similar to that of the original state.
2. When the frequency increases, the relative displacement between the male and female parts tends to follow the excitation frequency, so that the change of the connector resistances varies synchronously. At the two resonances, both the relative displacement and the connector resistance increase significantly, which is found by both experimental and theoretical analysis.

The relative displacement between the male and female parts causes the periodic occurrence of contact gaps between the spring and other connector parts, which changes the connector resistance. According to the time responses, the gaps in the steady state condition are dependent upon the relative displacement between the male and female parts.

NOMENCLATURE

d	The relative displacement between the female and male parts at the contact surfaces, equaling to $\|U_4 - U_1\|$
F_{ri}	The contact force for the ith repeated section of contact spring in radial direction, having two components in x-direction (F_{xi}) and y-direction (F_{yi})
k_e	The equivalent spring constant for the simplified two-dimensional model
M_i	The magnitude of the motion at the certain position of the connector system
R	Radius of the male part of connector
R_C	Connector resistance
r_i	The radial displacement of the ith repeated section of contact spring from steady state position
U_0	The motion at fixture, equals to $M_0\angle\phi_0$
U_1	The motion at the female part, equals to $M_1\angle\phi_1$
U_2	The motion at the right end of male part, equals to $M_2\angle\phi_2$
U_3	The motion at the midpoint of cable, equals to $M_3\angle\phi_3$
U_4	The motion at the male part, equals to $M_4\angle\phi_4$
α_i	The angle from the direction of vibration to the radial direction of the ith repeated section of contact spring

ΔR_C The temporary changes in connector resistance during vibration
ϕ_i The phase shift of the motion at certain position of the connector system

ACKNOWLEDGMENT

This work has been funded by LS Cable Company, Ltd. Without their strong support, this project could not have happened.

REFERENCES

Angadi, S. V., Jackson, R. L., Choe, S., Flowers, G. T., Lee, B., Liang, Z. (2012). A multiphysics finite element model of a 35A automotive connector including multiscale rough surface contact. *Journal of Electronic Packaging* 134(1):01001.

Carvou, E., Jemaa, N. B. (2007). Time and level analysis of contact voltage intermittences induced by fretting in power connector. In: *Proceedings of 53rd IEEE Holm Conference on Electrical Contacts*, pp. 211–215.

Carvou, E., Jemaa, N. B. (2009). Statistical study of voltage fluctuations in power connectors during fretting vibration. *IEEE Transactions on Components and Packaging Technologies* 32(2):268–272.

Chen, C., Flowers, G. T., Bozack, M., Suhling, J. (2009). Modeling and analysis of a connector system for the prediction of vibration-induced fretting degradation. In: *Proceedings of 55th IEEE Holm Conference on Electrical Contacts*, pp. 131–137.

Ervin, E. K., Wickert, J. A. (2007). Repetitive impact response of a beam structure subjected to harmonic base excitation. *Journal of Sound and Vibration* 307(1–2): 2–19.

Fu, R., Choe, S., Jackson, R. L., Flowers, G. T., Bozack, M. J., Zhong, L., Kim, D. (2012). Vibration-induced changes in the contact resistance of high power electrical connectors for hybrid vehicles. *IEEE Transactions on Components, Packaging and Manufacturing Technology* 2(2):185–193.

Hubner-Obenland, F., Minuth, J. (1999). A new test equipment for high dynamic real-time measuring of contact resistances. In: *Proceedings of 45th IEEE Holm Conference on Electrical Contacts*, pp. 193–202.

Jemaa, N. B. (2002). Contacts conduction and switching in DC levels. In: *Proceedings of 48th IEEE Holm Conference on Electrical Contacts*, pp. 1–15.

Kopanski, J. J. (1998). Intermittent-contact scanning capacitance microscope for lithographic overlay measurement. *Applied Physics Letters* 72(19):2469–2471.

Malucci, R. D. (2000). Possible mechanism for observed dynamic resistance. In: *Proceedings of 46th IEEE Holm Conference on Electrical Contacts*, pp. 254–267.

Maul, C., McBride, J. W. (2002). A model to describe intermittency phenomena in electrical connectors. In: *Proceedings of 48th IEEE Holm Conference on Electrical Contacts*, pp. 165–174.

Maul, C., McBride, J. W., Swingler, J. (2001). Intermittency phenomena in electrical connectors. *IEEE Transactions on Components and Packaging Technologies* 24(3):370–377.

McBride, J. W. (1989). Electrical contact bounce in medium-duty contacts. In: *Proceedings of 34th IEEE Holm Conference on Electrical Contacts*, pp. 141–149.

Murrel, S. R., McCarthy, S. L. (1997). Intermittence detection in fretting corrosion studies of electrical contacts. In: *Proceedings of 43rd IEEE Holm Conference on Electrical Contacts*, pp. 1–6.

Polchow, J. R., Angadi, S. V., Jackson, R. L., Choe, S., Flowers, G. T., Lee, B., Zhong, L. (2010). A multi-physics finite element analysis of round pin high power connectors. In: *Proceedings of 56th IEEE Holm Conference on Electrical Contacts*, pp. 1–9.

Skinner, D. W. (1975). Intermittent opens in electrical contacts caused by mechanically induced contact motion. *IEEE Transactions on Parts, Hybrids, and Packaging* 11(1):72–76.

Spitas, C., Spitas, V. (2007). A FEM study of the bending strength of circular fillet gear teeth compared to trochoidal fillets produced with enlarged cutter tip radius. *Mechanics Based Design Of Structures And Machines* 35(1):59–73.

Varenberg, M., Etsion, I., Halperin, G. (2004). Slip index: A new unified approach to fretting. *Tribology Letters* 17(3):569–573.

Waterhouse, R. B. (1972). *Fretting Corrosion*. Oxford: Pergamon.

Xie, F., Flowers, G. T., Chen, C., Bozack, M., Suhling, J., Rickett, B. I., Malucci, R. D., Manlapaz, C. (2009). Analysis and prediction of vibration-induced fretting motion in a blade/receptacle connector pair. *IEEE Transactions on Components and Packaging Technologies* 32(3):585–592.

Yan, S., Eiber, A., Schiehlen, W. (2005). Interaction between electrical and mechanical components in hand-held electrical tools. *Mechanics Based Design of Structures and Machines* 33(3–4):271–292.

Zhai, G., Fan, W., Liang, W. (2006). Study on contact resistance dynamic characteristics of space electromagnetic relay. In: *IMACS Multi Conference on Computational Engineering in System Applications*, pp. 1074–1081.